3910–3918 *Nucleic Acids Research, 2001, Vol. 29, No. 19*

Modelling ion binding to AA platform motifs in RNA: a continuum solvent study including conformational adaptation

Carmen Burkhardt and Martin Zacharias*

AG Theoretische Biophysik, Institut für Molekulare Biotechnologie, Beutenbergstrasse 11, D-07745 Jena, Germany

Received July 8, 2001; Revised and Accepted August 17, 2001

ABSTRACT

Binding of monovalent and divalent cations to two adenine–adenine platform structures from the *Tetrahymena* group I intron ribozyme has been studied using continuum solvent models based on the generalised Born and the finite-difference Poisson–Boltzmann approaches. The adenine–adenine platform RNA motif forms an experimentally characterised monovalent ion binding site important for ribozyme folding and function. Qualitative agreement between calculated and experimental ion placements and binding selectivity was obtained. The inclusion of solvation effects turned out to be important to obtain low energy structures and ion binding placements in agreement with the experiment. The calculations indicate that differences in solvation of the isolated ions contribute to the calculated ion binding preference. However, Coulomb attraction and van der Waals interactions due to ion size differences and RNA conformational adaptation also influence the calculated ion binding affinity. The calculated alkali ion binding selectivity for both platforms followed the order $K^+ > Na^+ > Rb^+ > Cs^+ > Li^+$ (Eisenman series VI) in the case of allowing RNA conformational relaxation during docking. With rigid RNA an Eisenman series V was obtained ($K^+ > Rb^+ > Na^+ > Cs^+ > Li^+$). Systematic energy minimisation docking simulations starting from several hundred initial placements of potassium ions on the surface of platform containing RNA fragments identified a coordination geometry in agreement with the experiment as the lowest energy binding site. The approach could be helpful to identify putative ion binding sites in nucleic acid structures determined at low resolution or with experimental methods that do not allow identification of ion binding sites.

INTRODUCTION

Folding of nucleic acid molecules into complex three-dimensional structures requires the association of counter ions to compensate for the electrostatic repulsion between negatively charged phosphate groups. Apart from non-specific accumulation of a diffuse counter ion atmosphere, site-specific divalent and monovalent metal ion binding can be required for the function and stability of folded nucleic acids (1–11). Over the past few years a rapidly growing number of experimental nucleic acid structures and complexes with proteins and other ligands have been determined by NMR spectroscopy and X-ray crystallography (9,12,13). In a number of high resolution crystallographic studies, ion binding positions could also be identified. Examples of crystallographically characterised monovalent metal ion binding sites are adenine–adenine (AA) platform motifs in the *Tetrahymena* group I intron (5–8). These motifs contain a non-canonical pseudo-base pair formed by two consecutive adenine nucleotides in one strand. Formation of one of these pseudo-base pairs creates an interface (in the RNA minor groove) that interacts with a GAAA tetraloop (G, guanine; A, adenine) at the end of another helix (the P4 helix) to stabilise the three-dimensional fold of the P4-P6 ribozyme domain (5,6). Biochemical and X-ray crystallographic studies (8) indicate that potassium ions are preferentially bound at a binding pocket near the AA pseudo-base pairs. In the case of the AA platform, which is part of the tetraloop acceptor, the ion binding site does not participate in direct tertiary contacts. Instead, it is located at a side of the RNA helix facing away from the region in contact with the tetraloop (5–8). Presumably, its function is to stabilise the AA platform structure such that it allows optimal contact with the GAAA tetraloop. The ion binding properties of AA platform structures in the P4-P6 ribozyme domain have been elucidated by comparing electron density maps in the presence of potassium (K^+) and thallium (Tl^+), a cation of similar size and hydration properties as potassium. These studies revealed three binding sites that corresponded to the known AA platform motifs in the P4-P6 domain (8). Caesium instead of Tl^+ produced weaker difference electron density peaks at these sites indicating weaker ion binding and soaking experiments with divalent ions such as Mn^{2+} did not yield any additional electron density at the platform motif (8). The monovalent ion binding site near the tetraloop acceptor and its importance for proper RNA folding was also confirmed biochemically using nucleotide analogue interference mapping (8).

Structural information on specific ion binding to nucleic acids does not allow a direct insight into the driving forces and energetic contributions that determine ion binding affinity and

*To whom correspondence should be addressed. Tel: +49 3641 656209; Fax: +49 3641 656495; Email: zacharia@imb-jena.de

specificity to structural motifs. However, such an understanding of why certain structural motifs in nucleic acids are specific ion binding sites could be helpful to better understand the mechanism of RNA structure formation and function. Computational approaches such as molecular dynamics simulations on ions in complex with nucleic acids including explicit water molecules are useful to study nucleic acid dynamics and how it is influenced by the type and concentration of ions (14–21). However, due to the computational demand such studies are limited to small time scales (nanoseconds), allowing only limited motions of associated ions. The evaluation of relative ion binding free energies requires determination of a thermodynamic average over solute and all solvent degrees of freedom during thermodynamic integration or perturbation calculations for which convergence is difficult to achieve (22,23).

In the present study a computational approach using a generalised Born (GB) solvation model (24–29) and including RNA conformational flexibility has been employed to investigate the binding of various ions to experimentally determined AA platform structures. The GB method allows an approximate calculation of the average solvent polarisation due to solute charges. It has recently been successfully applied in systematic conformational search studies on trinucleotide loops in DNA (30), molecular dynamics simulations of hairpin loops in RNA (31–33) and on regular double-stranded DNA and RNA resulting in trajectories in good agreement with simulations in the presence of explicit solvent (34). In the present ion–RNA docking study the energy minimised ion–RNA complexes were further evaluated with a non-linear finite-difference Poisson–Boltzmann approach (35). The calculations reproduce the experimentally known preference for monovalent ions, especially potassium, to AA platform motifs. Furthermore, systematic multi-start energy minimisations from positions at the surface of AA platform containing RNA fragments revealed positions close to experiment as lowest energy binding sites. A decomposition of the calculated binding energies allows elucidation of various energetic and solvation contributions as well as the influence of RNA conformational relaxation on ion binding preference.

Besides better understanding of the energetics of ion–RNA binding, the present approach might also be useful to identify putative binding sites in experimental structures determined only at low resolution or with methods that do not allow easy determination of ion binding positions (e.g. NMR spectroscopy).

MATERIALS AND METHODS

Energy minimisation and docking of ions to RNA

Energy minimisation (EM) and ion docking calculations were performed using a modified version of the Jumna (Junction minimisation of nucleic acids) program (36) and the Amber4.1 force field (37). The Lennard–Jones parameters for ions are from Aqvist (38). In the Jumna program, helicoidal coordinates (three translational variables: Xdisp, Ydisp and Rise; and three rotational variables: Inclination, Tip and Twist) are used to place 3′-monophosphate nucleotides in space. In addition, single bond torsion and valence angles are used to describe the internal nucleotide flexibility. Except for the connection between each nucleotide, all bond lengths are assumed to be fixed at their optimum values. This description of nucleic acid conformation allows a very efficient energy minimisation down to small residual gradients (energy changes $<10^{-7}$ kcal mol^{-1} per step) in less than ~2000 EM steps. Such calculations can require many more EM steps and are much more time consuming when using, for example, Cartesian coordinates. The energy function for energy minimisation consists of valence angle and dihedral angle contributions (ΔE_{AT}) and non-bonded Lennard–Jones (ΔE_{LJ}) and electrostatic terms. No cutoff was used for the non-bonded interactions.

$$
\begin{aligned}
V = {} & \Sigma_{angles} \tfrac{1}{2} K_\theta (\theta - \theta_o)^2 \\
& + \Sigma_{torsions} K_\tau [1 + \cos(n\tau - \delta)] \\
& + \Sigma_{i<j} (C_{12} r_{ij}^{-12} - C_6 r_{ij}^{-6}) \\
& + \Sigma_{i<j} q_i q_j (r_{ij})^{-1} \\
& - \tfrac{1}{2} (1 - \varepsilon_w^{-1}) \Sigma_{i,j} q_i q_j (r^2_{ij} + \alpha^2_{ij} \exp[-r^2_{ij}/4\alpha^2_{ij}])^{-1/2}
\end{aligned}
$$

During EM electrostatic contributions were calculated using the GB model (24–26). In the GB model electrostatic solvation or reaction field contributions (ΔE_{reGB}) due to differences in the assigned dielectric constants for the molecule ($\varepsilon = 1.0$) and surrounding aqueous solvent ($\varepsilon_w = 78.0$) are calculated from the charge and atom distribution in the molecule. An interior dielectric of $\varepsilon = 1.0$ was used since flexible degrees of freedom of the RNA have been included explicitly. The α_{ij} were calculated using the pairwise descreening approximation described by Hawkins *et al.* (25,26). A set of atomic radii close to the Parse set (39) was used with hydrogen radius (in Å) of $R_H = 1.0$, $R_C = 1.7$, $R_N = 1.6$, $R_O = 1.5$ and $R_P = 2.0$, respectively. The descreening parameters were $S_H = 0.82$, $S_C = 0.77$, $S_N = 0.77$, $S_O = 0.83$ and $S_P = 0.84$, respectively, using a radius offset parameter of –0.12 Å. For RNA and RNA in complex with monovalent ions these parameters give a very reasonable correlation to reaction field energies calculated with a finite-difference solution of the Poisson equation (FDPB) using the UHBD program (40) and the same set of atomic radii. To check the effect of an alternative choice of GB parameters for some calculations, a set of modified Bondi parameters (41) used by Tsui and Case (34) in MD simulations of RNA and DNA has also been applied. The Born radii used for each ion during docking to calculate solvation free energies are not identical to the ion van der Waals radii in the present model but have been chosen such that the experimental free energies of hydration are reproduced including a surface area dependent non-polar cavity term. In order to reduce grid errors in the calculation of relative ion binding energies with the FDPB approach, ion solvation energies obtained under the same grid conditions as for the calculations on RNA–ion complexes served as reference [experimental hydration free energies are given in parentheses according to Burgess (42), in kcal mol^{-1}]: K^+, –80.3 (–80.5); Na^+, –98.1 (–98.2); Rb^+, –75.6 (–75.5); Cs^+, –67.8 (67.8); Li^+, –122.1 (–122.1); Mg^{2+}, –455.1 (–455.5); Ca^{2+}, –380.7 (–380.8).

Surface area dependent non-polar solvation contributions (ΔE_{SASA}) were evaluated from the accessible surface area with $\gamma = 0.0055$ kcal mol^{-1} Å^{-2} (39). This term was only calculated for the final energy minimised structures since it varies very little between the EM position and an initial placement of the ion at the surface of the RNA close to the binding site (less than ~0.1 kcal mol^{-1}). The total energy of a conformer (ΔE_{totPB} or ΔE_{totGB}) is given as a sum of Coulomb (ΔE_{Coul}), Lennard–Jones

(ΔE_{LJ}), valence and torsion angle (ΔE_{TA}), electrostatic solvation (ΔE_{rePB} or ΔE_{reGB}) and non-polar solvation contributions (ΔE_{SASA}).

Generation of adenine–adenine platform start structures

A systematic analysis of ion binding to the complete P4-P6 ribozyme domain including energy minimisation of the RNA coordinates and many different ion types and initial ion placements is computationally not feasible. Therefore, in the present computational studies two RNA fragments containing either the so-called J6a/6b or the J6/6a AA platform motifs [nomenclature according to Basu *et al.* (8)] were cut out of the P4-P6 domain X-ray structure (5,6) and served as start structures for energy minimisation and docking studies. In the case of the J6a/6b platform the RNA fragment contained nucleotides 221–229 (first strand: 5′-UCCUAAGUC) and 245–252 (second strand: 5′-GAUAUGGA) according to the numbering in the P4-P6 domain structure (5,6). The AA platform pseudo-base pair is formed by nucleotides A_{225} and A_{226}. A fragment of similar size was used in the case of the J6/6a motif consisting of nucleotides 215–223 (first strand: 5′-GCCAAGUCC, with A_{218} and A_{219} forming the AA platform), nucleotides 103–105 (second strand: 5′-GAA, pairing with nucleotides 215–217) and nucleotides 250–253 (third strand: 5′-GGAU, Watson–Crick pairing with nucleotides 220–223 of the first strand). For simplicity, in the following, the two AA platforms are termed AA1 (J6a/6b) and AA2 (J6/6a) platform motifs, respectively.

Ion docking was performed by placing the selected ion at a position close to the experimentally described coordination site (8) followed by energy minimisation including solvation within the GB approach and either rigid or fully flexible RNA. For systematic docking studies starting from various positions at the surface of the RNA molecule a modification of the Shrake and Rupley solvent accessible surface algorithm (43) was used with a probe radius corresponding to the potassium ion radius generating ~800 accessible surface start sites. Subsequent energy minimisation keeping the RNA rigid identified a number of putative ion binding sites within an energy threshold of the lowest energy site. A subset of low energy ion binding sites were further minimised including conformational flexibility of the RNA.

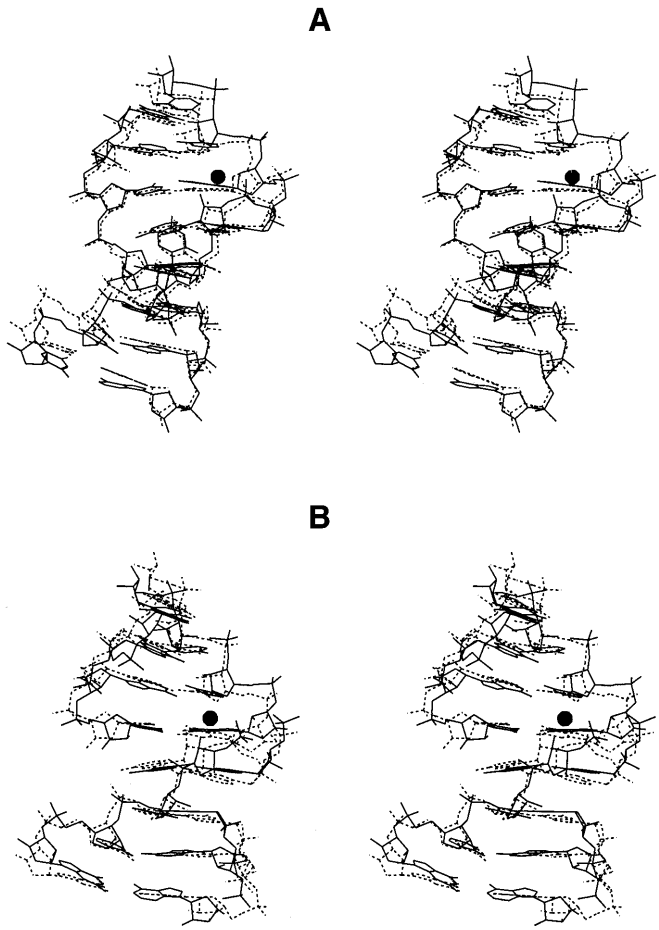

Figure 1. Stereo views of the superposition of AA platform containing RNA fragments (continuous line) energy minimised with a bound K^+ ion (indicated as a sphere) at a position compatible with the experimentally observed coordination geometry (8) onto the corresponding crystallographic *Tetrahymena* ribozyme P4-P6 domain structure (PDB accession no. 1gid, reference 5, dashed line). (**A**) RNA fragment with the AA1 platform corresponding to nucleotides 221–229 (first strand) and 245–252 (second strand), respectively. (**B**) AA platform 2 (AA2) containing fragment (continuous line) with a bound K^+ superimposed on nucleotides 215–223 (first strand), nucleotides 103–105 (second strand pairing with nucleotides 215–217) and nucleotides 250–253 (third strand, pairing with nucleotides 220–223 of the first strand) from the crystal structure (dashed line).

RESULTS

Docking monovalent and divalent cations to AA platform structures

Energy minimisation of cations (K^+, Na^+, Rb^+, Cs^+, Li^+, Ca^{2+} and Mg^{2+}) placed approximately at the known AA platform binding sites (8) resulted in geometries compatible with the experimentally observed ion coordination. This coordination is characterised by ion contacts (distance <3.5 Å) to O6 and N7 of G_{227} (AA1 platform) or G_{220} (AA2 platform), ribose O2′ of A_{225} (AA1) or A_{218} (AA2) and the phosphate group of A_{226} (AA1) or A_{219} in the case of the AA2 platform (8). The energy minimised flexible RNA structures stayed for all ion complexes close to the experimental start structures (Fig. 1) with heavy atom root mean square deviations (r.m.s.d.) of <1.6 Å from the corresponding RNA start structures, respectively. In the absence of ions EM structures showed an r.m.s.d. of 1.0 and 2.3 Å for AA1 and AA2 platforms, respectively. Docking of Mg^{2+} required the inclusion of distance constraints to keep the ion at the binding site (Table 1 legend). The distance constraints approximately represent the ion–RNA contacts found experimentally (see above and 8). Without these constraints the Mg^{2+} ion moves to the nearest phosphate oxygen a few angstroms apart from the potassium binding site. The inclusion of the same distance constraints was necessary in the case of both Mg^{2+} and Ca^{2+} docked to rigid RNA. For all monovalent ions docked to rigid RNA the resulting energy minimised positions deviated from those obtained using flexible RNA by <1 Å (after best superposition of the RNAs). The largest differences in ion placement between rigid and flexible docking were found in the case of Li^+ and Cs^+ ions.

Calculation of relative ion binding energies

Ion binding energies were calculated by subtracting the calculated energies for the unbound energy minimised RNA and the

Table 1. Calculated ranking of ion binding to AA platform motifs

Ion	ΔE_{bindPB}	ΔE_{bindGB}		ΔE_{bindPB}	ΔE_{bindGB}
	Flexible docking		$\Delta\Delta E_{salt}$	Rigid docking	
AAP1 complex					
K^+	–20.3 (–18.2)	–21.1 (–16.6)	3.9	–16.3	–18.9
Na^+	–19.6 (–18.0)	–21.4 (–17.5)	3.5	–13.7	–16.3
Rb^+	–17.9 (–15.3)	–19.8 (–15.2)	3.9	–15.3	–18.7
Cs^+	–14.6 (–12.1)	–18.0 (–13.3)	4.7	–13.5	–17.0
Li^+	–14.5 (–10.2)	–18.0 (–15.4)	3.5	–2.3	–11.0
Mg^{2+}	14.1 (19.8)	–2.4 (2.3)	8.4	57.8[a]	18.0[a]
Ca^{2+}	2.9 (3.6)	–10.7 (–3.9)	8.6	20.8[a]	3.3[a]
AAP2 complex					
K^+	–20.9	–18.7	4.1	–14.3	–17.7
Na^+	–19.6	–18.4	3.8	–10.7	–14.7
Rb^+	–18.4	–17.6	4.2	–13.7	–17.6
Cs^+	–12.3	–17.2	4.6	–12.2	–16.4
Li^+	–10.1	–14.2	3.7	–2.0	–9.8
Mg^{2+}	21.4[a]	2.4[a]	8.5	52.8[a]	17.6[a]
Ca^{2+}	–3.7	–8.0	8.0	21.9[a]	4.9[a]

Calculated relative ion binding energies are given in kcal mol^{-1} (see text for details). ΔE_{bindPB} and ΔE_{bindGB} correspond to the binding energies using the FDPB or GB methods, respectively, to calculate electrostatic solvation contributions for binding to flexible RNA (columns 2 and 3) and rigid RNA (columns 5 and 6). Values in parentheses are calculated binding energies obtained using the modified Bondi (41) atom radii and screening parameters described by Tsui and Case (34). Column 4 gives the change in calculated ion binding energy for binding to flexible RNA at 150 mM bulk salt concentration (relative to 0 mM) solving the non-linear finite-difference PB equation.

[a]For docking Mg^{2+} and Ca^{2+} to rigid RNA the inclusion of distance constraints (range 2.5–3.5 Å) between ion and O2′ of A_{225} (A_{218} in the case of AA2) and between ion and O6/N7, respectively, of G_{227} (G_{220} in the case of AA2) was necessary to keep the ion close to the experimentally observed coordination site.

calculated solvation free energies of the isolated ions from the energy of the energy minimised complex. The unbound reference states for the binding energy calculations are the AA1- and AA2-containing RNA fragments, respectively, that were energy minimised in the absence of ions starting from the AA platform conformation found in the X-ray structure (5–7). The possibility that the RNA adopts a different conformation in the absence of a monovalent ion that is separated by an energy barrier from the form in the crystal structure as suggested by NMR spectroscopy of the isolated platform motif (44) is not accounted for. Under the assumption that the stability of such a 'free' RNA structure is not affected by ion type it should not influence the relative ranking of ion binding to the platform motif. In this sense the calculated ion binding energies are relative binding energies with respect to a reference conformation close to the form observed in the crystal structure. Other contributions that are not included and that may also influence absolute ion binding energies (but much less so relative binding energies) are the reduction in RNA conformational flexibility and ion translational degrees of freedom that both disfavour ion binding.

For both AA platform motifs and for rigid and flexible docking the calculated monovalent cation binding energies were negative (Table 1). The results for both GB and FDPB approaches are similar although in the case of the AA1 structure the GB model predicts Na^+ to bind slightly better than K^+. Using an alternative set of GB parameters and atomic radii derived by Tsui and Case (34) based on the set by Bondi (41) resulted in qualitatively similar ranking for ion binding. For divalent ions, especially Mg^{2+}, the calculated binding energies were much less favourable or positive compared to monovalent ions. In addition, the agreement of GB and FDPB results was worse compared to binding energies for monovalent ions.

For docking to rigid RNA (energy minimised in the absence of ions) calculated monovalent ion binding energies were still negative but ~2–9 kcal mol^{-1} less favourable than for docking to fully flexible RNA. The influence of conformational adaptation during ion binding calculations was larger for smaller monovalent (Li^+ and Na^+) ions and divalent ions than for larger monovalent ions such as K^+, Rb^+ and Cs^+.

Except for the AA1 platform and evaluation with the GB model the calculations on both rigid and flexible RNA platforms predict binding of potassium as more favourable than other ions (the predicted potassium selectivity is slightly larger in the case of docking to rigid RNA; Table 1). Although no quantitative experimental data on the relative ion binding preference to AA platforms is available, the predicted preference of monovalent, especially potassium, ions is in qualitative agreement with experiments by Basu *et al.* (8). Inspection of the energetic contributions in Table 2 indicates that the calculated negative binding energies at the platform sites for monovalent ions are primarily due to electrostatic interactions. For all monovalent

Table 2. Calculated contributions to ion–AA platform binding

Ion	ΔE_{ElecPB}	ΔE_{ElecGB}	ΔE_{rePB}	ΔE_{reGB}	ΔE_{Coul}	ΔE_{TA}	ΔE_{LJ}	ΔE_{SASA}	ΔE_{LJLN}	ΔE_{CoulLN}
Docking to flexible AA1-RNA										
K^+	–25.6	–26.4	549.3	548.5	–574.9	–0.1	7.4	–2.1	8.6	–586.8
Na^+	–22.4	–24.2	560.3	558.6	–582.8	0.1	4.4	–1.7	7.2	–613.6
Rb^+	–23.6	–25.6	547.5	545.5	–571.1	–0.1	8.0	–2.2	8.6	–577.1
Cs^+	–20.9	–24.3	542.0	538.6	–562.8	0.0	8.7	–2.4	8.2	–563.1
Li^+	–13.5	–17.2	578.1	574.4	–591.6	–1.0	1.5	–1.5	5.3	–631.3
Mg^{2+}	4.8	–11.8	1179.7	1163.1	–1175.9	1.5	8.8	–0.9	10.0	–1214.1
Ca^{2+}	–7.6	–21.1	1187.6	1174.0	–1195.2	1.4	10.4	–1.4	9.7	–1232.9
Docking to rigid AA1-RNA										
K^+	–19.3	–22.0	551.0	548.3	–570.3	0.0	5.0	–2.0	5.0	–570.3
Na^+	–15.4	–18.0	566.9	564.3	–582.3	0.0	3.2	–1.6	3.2	–582.4
Rb^+	–19.5	–22.9	547.1	543.7	–566.6	0.0	6.3	–2.1	6.3	–566.6
Cs^+	–21.7	–25.1	540.7	537.2	–562.3	0.0	10.6	–2.4	10.6	–562.3
Li^+	–3.1	–11.8	587.7	579.0	–590.9	0.0	2.1	–1.3	2.1	–590.9
Mg^{2+}	60.8	20.9	1166.7	1126.9	–1105.9	0.0	–2.0	–0.9	–2.0	–1105.9
Ca^{2+}	23.8	6.3	1149.1	1131.6	–1125.2	0.0	–1.7	–1.4	–1.7	–1125.3
Docking to flexible AA2-RNA										
K^+	–30.6	–28.4	493.7	495.9	–524.3	–0.7	12.3	–1.8	8.2	–564.5
Na^+	–27.8	–26.6	495.7	496.9	–523.5	–0.1	9.7	–1.5	6.4	–590.1
Rb^+	–28.2	–27.4	494.7	495.5	–522.9	–0.8	12.6	–1.8	8.1	–555.2
Cs^+	–17.6	–22.6	512.9	508.0	–530.5	0.2	7.5	–2.4	7.5	–539.3
Li^+	–16.4	–20.6	503.7	499.6	–520.1	–1.4	8.9	–1.2	4.2	–603.7
Mg^{2+}	14.4	–4.7	1135.7	1116.6	–1121.3	3.2	4.7	–0.8	6.1	–1146.6
Ca^{2+}	–18.5	–22.8	1094.0	1089.8	–1112.5	1.1	14.8	–1.2	9.2	–1185.8
Docking to rigid AA2-RNA										
K^+	–16.8	–20.3	526.9	523.4	–543.7	0.0	4.5	–2.0	4.6	–543.7
Na^+	–11.6	–15.6	539.4	535.4	–551.0	0.0	2.4	–1.6	2.4	–551.0
Rb^+	–17.1	–21.1	523.7	519.7	–540.8	0.0	5.6	–2.1	5.6	–540.8
Cs^+	–18.3	–22.6	518.3	514.0	–536.7	0.0	8.5	–2.4	8.5	–536.7
Li^+	–2.9	–10.7	557.1	549.4	–560.1	0.0	2.2	–1.3	2.2	–560.1
Mg^{2+}	55.5	20.3	1109.1	1073.9	–1053.6	0.0	–1.7	–0.9	–1.7	–1053.6
Ca^{2+}	25.1	8.1	1106.8	1089.8	–1081.7	0.0	–1.8	–1.4	–1.8	–1081.7

Energetic contributions are given in kcal mol^{-1}. Changes in energetic contributions were obtained by subtracting the energies of the isolated components from the energy of ion–RNA complexes. ΔE_{ElecPB} and ΔE_{ElecGB}, change of total electrostatic energy using FDPB or GB approaches, respectively. ΔE_{rePB} and ΔE_{reGB}, change of electrostatic solvation; ΔE_{Coul}, coulomb contribution to binding energy; $\Delta\Delta E_{TA}$, change in valence and torsion angle contributions of the platform structures upon complex formation. ΔE_{LJ}, ΔE_{SASA}, ΔE_{LJLN} and ΔE_{CoulLN}, change in total Lennard–Jones, surface area dependent cavity contribution, ion–RNA Lennard–Jones interaction and ion–RNA coulomb interaction, respectively, upon complex formation.

ions the attractive Coulomb contribution at the binding site was found to outbalance the (positive) ion and RNA desolvation penalty. In the case of divalent ions the total electrostatic contributions only slightly favour (Ca^{2+}) or overall disfavour binding (Mg^{2+}). The calculated differences in electrostatic solvation between the various RNA–ion complexes were smaller than the differences in solvation of the isolated ions (see Materials and Methods for the ion solvation free energies). This tendency is more strongly reflected in the case of rigid RNA–ion docking complexes which contribute to overall slightly smaller ion binding energy differences if one accounts for conformational adaptation during docking. No rule such that, for example, the calculated differential ion binding properties are simply determined by the hydration properties of the isolated ion was observed (such a rule would always favour less well hydrated ions such as Rb^+ and Cs^+ compared to K^+ or Na^+). According to Eisenman (45,46) selective binding of alkali cations to binding sites, for example in glass electrodes or membranes, is due to an asymmetry between ion–site and ion–water interactions. Specifically, for ion selective

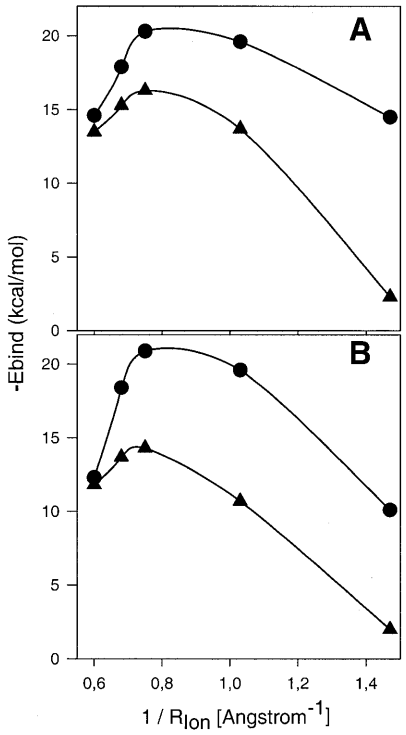

Figure 2. Plot of the calculated relative ion binding energy versus the reciprocal ion (van der Waals) radius for the (**A**) AA1- and the (**B**) AA2-containing RNA fragments with various alkali ions bound at the experimentally observed coordination site. The reciprocal ions radii (*x*-axis) follow the order Cs^+, Rb^+, K^+, Na^+ and Li^+, with results for docking to fully flexible RNA represented by dots and for rigid RNA (energy minimised before ion docking in the absence of a bound ion) represented by triangles.

site-specific binding the ion–site interactions must fall off as a lower power of ion radius than the ion hydration properties, (46) giving rise to a convex shape of the ion binding energies plotted versus ion radius (or the reciprocal ion radius). Such a shape was also found for the calculated energies of monovalent ion binding to the AA platform structures versus the reciprocal ion radius (Fig. 2). The predicted maxima of ion binding for a hypothetical ion with a radius between potassium and sodium ion radii were similar for both AA platforms (Fig. 2). The plots also illustrate that inclusion of RNA flexibility during ion docking makes a favourable contribution to ion binding and, in addition, shifts the predicted ion selectivity for both platforms from an Eisenman series V (relative binding energies follow the order $K^+ > Rb^+ > Na^+ > Cs^+ > Li^+$) to VI ($K^+ > Na^+ > Rb^+ > Cs^+ > Li^+$).

For the less well hydrated larger monovalent ions such as Rb^+ and Cs^+, the overall change in reaction field energy upon complex formation is less positive than for K^+. However, compared to Rb^+ and Cs^+, more negative Coulomb contributions favour binding of K^+ at the platform binding site. The electrostatic favouritism of potassium over other ions is due to a balance between ion–RNA Coulomb attraction, small changes in RNA internal interactions and changes in solvation. Beside electrostatic contributions, Lennard–Jones (van der Waals) interactions disfavour ion binding. This positive van der Waals contribution is due to the strong electrostatic attraction of the ions that leads to a small increase in the Lennard–Jones term. For hard ions (e.g. K^+) this contribution appears to be more positive than for softer ions (e.g. Na^+) reducing the overall preference for potassium. Calculated changes in bond angle and torsion angle terms as well as surface area dependent non-polar solvation contributions add ~1 kcal mol^{-1} to the relative binding preference. This result is compatible with the relatively small conformational changes in the RNA observed during flexible docking.

Comparison of calculated binding energies for rigid and flexible docking indicates that inclusion of flexibility results in more negative ion binding energies. Inclusion of RNA conformational adaptation significantly enhances the Coulomb attraction between ion and RNA which is, however, partially compensated by an increase in RNA internal energy (Table 2). The largest conformational as well as energetic changes were observed for divalent and smaller alkali ions such as Li^+ and Na^+. Inclusion of RNA conformational flexibility had a greater effect in the case of the AA2 platform. Presumably because this RNA fragment consisted of three strands it also had a greater capacity for conformational adaptation than the AA1 platform fragment. Inclusion of RNA flexibility partially compensates for the calculated repulsion (due to desolvation) of divalent ions at the platform sites.

During energy minimisation, non-specific effects of the surrounding ion atmosphere have not been included because docking studies using, for example, the non-linear FDPB method to account for non-specific salt effects are computationally not feasible. However, under the assumption that the energy minimum position does not depend significantly on the salt concentration, the salt dependence can be calculated by solving the non-linear FDPB for the final energy minimised complexes at various bulk salt concentrations. Control calculations using the non-linear FDPB and small ion displacements from the position at the energy minimum resulted in very similar salt dependencies (data not shown). This result indicates that the energy minimum (ion) placement does not change dramatically upon changing the salt concentration and that the calculated dependence on the non-specific salt atmosphere is relatively insensitive to small misplacements of site specific bound ions. For all monovalent ions a similar reduction in ion binding energies upon increasing the bulk salt concentration was found (~3.5–4.5 kcal mol^{-1} upon addition of 150 mM bulk salt; see Table 1). This means that one needs a higher salt concentration to 'salt out' potassium compared to, for example, Cs^+ because potassium is predicted to bind more strongly at zero salt than Cs^+. A larger salt dependence was found for the binding of divalent cations (~8.5 kcal mol^{-1} upon addition of 150 mM salt) indicating that non-specific salt screening reduces divalent ion binding more dramatically than monovalent ion binding.

Energy minimisation starting from multiple positions at the RNA surface

Uniformly distributed docking start positions at the surface of the energy minimised unbound (apo-) AA1 and AA2 RNA fragments were systematically generated using the Shrake and Rupley method (43) with a probe radius that corresponded to the van der Waals radius of potassium (~800 positions on the surface of each molecule). Energy minimisation was performed with rigid RNA and yielded in both cases ~50 distinct energy minima. The large ratio between start positions

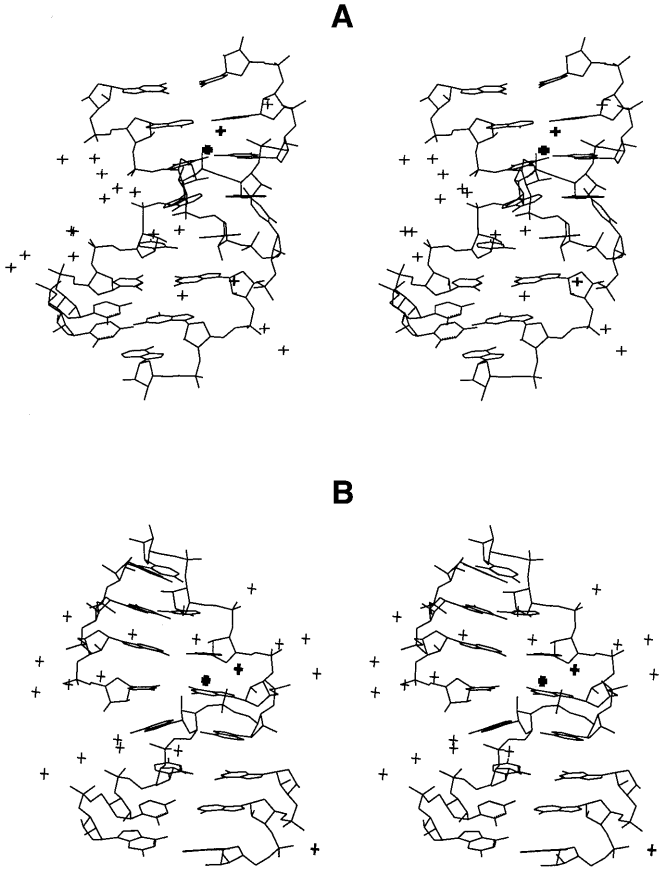

Figure 3. (**A**) Stereo view of the AA1 platform containing RNA fragment and 18 low energy ion binding sites (indicated by crosses) obtained after systematic docking by energy minimisation of ~800 evenly distributed K^+ ions at the surface of the RNA fragment. The three most favourable ion binding positions are indicated by an increased cross thickness. (**B**) Stereo view of the AA2 platform containing RNA fragment with the 18 most favourable calculated K^+ binding sites.

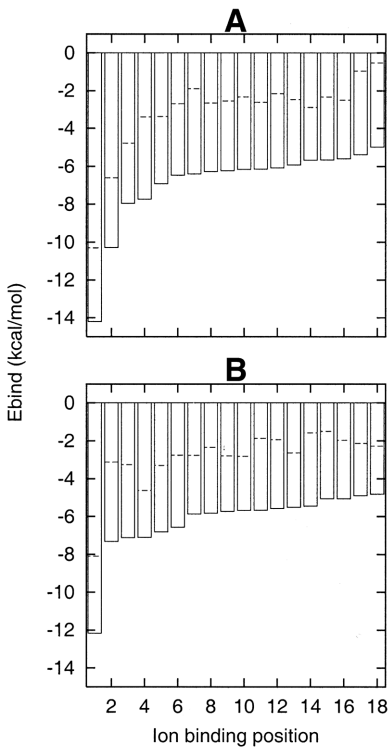

Figure 4. Calculated relative K^+ binding energies of the 18 most favourable ion binding positions obtained from systematic docking studies to RNA fragments containing the AA1 platform (**A**) and the AA2 platform (**B**), respectively. The most favourable binding energy (left most bar) was obtained for binding to the experimentally observed coordination site for both platform motifs. Binding energies were calculated by subtracting the ion–RNA complex energy from the energy of the isolated ion and the RNA (rigid RNA, non-polar solvation term not included). Electrostatic solvation contributions were calculated by solving the non-linear FDPB in the absence (continuous lines) and presence of 150 mM bulk salt (dashed lines).

and energy minima (~10:1; all minima were obtained several times starting form different start positions) indicates that the search is likely to cover most ion binding minima at the surface of both RNA molecules (the search took ~8 h on a SGI R12000 workstation). Most of the minima corresponded to ion placements close to a phosphate oxygen (Fig. 3). Some minima showed the potassium ion located near partially negatively charged (e.g. oxygen) atoms of nucleo-bases in the RNA grooves. The lowest energy minimum, however, was for both RNA molecules identical to the rigid RNA potassium complex obtained starting from a position close to the experimentally observed binding position (see above). Energy minimisation of the complexes with fully flexible RNA resulted in complexes identical to the docked complex obtained using flexible RNA described in the previous paragraphs. Interestingly, a significantly larger energy gap between first and second lowest energy ion binding position of ~5 kcal mol^{-1} (Fig. 4) than energy differences between higher ranked ion binding positions (mostly located at equivalent sites close to phosphate oxygens) was found. The observation that a relatively modest number of ion start positions is sufficient to find most putative ion binding energy minima on the RNA surface and the relatively large energy difference between the lowest energy binding positions (equivalent to the experimentally found ion binding sites) and alternative binding sites indicates that the approach could be useful for studies on other larger RNA molecules with specific but unknown binding sites.

DISCUSSION

The association of monovalent and divalent cations is essential for the proper folding and function of nucleic acids (4,7,10). Using NMR spectroscopy or X-ray crystallography at low resolution it is often difficult to determine the identity and exact localisation of ions bound to RNA and DNA structures. In addition, the physical basis for ion binding affinity and specificity, e.g. which interactions or energetic contributions determine ion binding preferences and how it is influenced by conformational adaptation, is not completely understood. The aim of the current study was to test the ability of an implicit solvation model based on the GB and FDPB approaches combined with an atomic resolution representation of the RNA to predict experimentally observed trends for ion binding at AA platform structures. The analysis of energetic contributions offers some insight into the mechanism of ion binding affinity and selectivity. In the present model the ion is represented as a Born sphere embedded in a continuum

solvent. The Born radii of the ions are adjusted such that calculated solvation free energies agree with experimentally observed free energies of ion hydration. The ion–RNA interaction consists of contributions given by the desolvation of ion (and RNA) upon complex formation and Coulomb interactions as well as Lennard–Jones interactions between ion and RNA. Additional indirect contributions are due to the inclusion of RNA conformational flexibility or adaptation upon ion binding that influences the RNA conformational energy. The hard or soft character of the ions is determined by the Lennard–Jones parameters. Although the model completely neglects the discrete nature of water molecules and more complex ion–RNA interaction (e.g. ion-specific electronic contributions that can not be described using a classical force field but require a quantum chemical treatment) the ion placements after energy minimisation and the calculated preference for monovalent, especially potassium, ion binding was in qualitative agreement with the experiment. The experimental data on ion binding to AA platform structures in the *Tetrahymena* group I intron ribozyme come from nucleotide analogue interference mapping and ribozyme activity measurements in the presence of various monovalent ions and analysis of difference electron densities for different RNA–ion complexes (8). These experiments allow only a qualitative comparison of experimentally observed ion preferences and calculated relative ion binding affinities. A convex shape for the calculated ion binding selectivity as a function of ion radius was found that is typical for an Eisenman selectivity series seen experimentally for alkali ion binding to glass electrodes and other alkali cation complexing agents (reviewed in 46).

Compared to explicit solvent methods the present approach is fast enough to allow systematic studies with several ions and many ion start placements, and at the same time to extract estimates for relative ion binding preferences. It is important to emphasise that although GB or FDPB approaches offer only an approximate description of aqueous solvation effects its inclusion during ion docking is, nevertheless, of critical importance for realistic ion binding predictions. For example, simple pair-wise electrostatic models, i.e. with a distance dependent effective dielectric constant, would always favour divalent metal ion binding over monovalent cation binding at any site with a negative electrostatic potential and do not give a convex shape for binding as a function of ion radius. This holds also for approaches that treat the ion as test charge in a pre-calculated electrostatic potential around a nucleic acid molecule that are, for example, applied in brownian dynamics calculations of ion diffusion (47). In addition, neglect of solvation during docking can result in binding energies that are much too negative and energy minimisation with a pair-wise electrostatic model can lead to unrealistic deformations of the nucleic acid structure (48,49). In contrast, inclusion of electrostatic solvation effects during EM of fully flexible RNA–ion complexes within the GB model resulted in structures close to the experimental start structure.

The calculated binding energies for divalent cations constraint to the binding pocket are considerably more positive than for monovalent ions. This result is in qualitative agreement with the experimental observation of specific monovalent metal ion binding to the AA platform motif (8). However, the large calculated difference between monovalent and divalent cation binding might also be due to the fact that in the case of divalent ions (in particular Mg^{2+}) the continuum solvent description is a more severe approximation than in the case of monovalent cations with a much weaker bound hydration shell. A possible extension of the present continuum solvent approach is to treat the first hydration shell of divalent cations explicitly during docking.

In the present analysis the unbound RNA platform reference structure for calculating binding energies corresponded to an energy minimum close to the conformation observed in the X-ray structure of the P4-P6 ribozyme domain (5–7). Structural studies on RNA fragments with the isolated 'free' AA platform motif indicate a conformation that differs from the form observed in the folded P4-P6 domain (44). It is likely that such a conformational transition affects the absolute ion binding affinity to the platform target motif. However, under the assumption that such an isolated platform structure is not differentially affected by different ion types, it does not influence the ranking of ion binding to the AA platform motif in the conformation found in the crystal structure. Additional contributions that are likely to affect absolute ion binding free energies and that have not been considered in the present study come from possible changes of RNA conformational flexibility upon ion binding and changes of translational degrees of freedom of bound versus free ions.

The present calculations indicate that monovalent ion binding to the AA platform motif is driven by electrostatic Coulomb attraction that is not completely balanced by an opposing desolvation penalty. Binding affinity and specificity is, however, also influenced by packing interactions that disfavour the binding especially of harder ions (e.g. K^+). In the case of divalent cations the desolvation penalty for binding to the binding pocket is much larger and either almost offsets the strong electrostatic attraction or results in an overall electrostatic repulsion at the particular site. Divalent cation binding can, however, still occur at other non-specific sites or pockets with a different geometry and smaller desolvation penalty.

Inclusion of conformational flexibility of the RNA upon ion binding leads to modest conformational changes and makes a favourable ion specific contribution if one uses platform structures energy minimised in the absence of ions as reference structure. The calculations indicate that inclusion of conformational relaxation can shift the alkali ion selectivity from an Eisenman series V in the case of rigid RNA to VI in the case of flexible RNA. Note that this computational result demonstrates the possible effect of RNA flexibility on ion binding affinity and specificity. Since real RNA is inherently flexible the calculated Eisenman series, in particular for rigid ion–RNA docking, may not be of biological relevance. The calculated conformational changes of the RNA upon ion docking are relatively modest (change in heavy atom r.m.s.d. ~1–1.5 Å). It is likely that for more flexible putative ion binding sites in nucleic acids conformational adaptation may have an even more significant effect on ion binding affinity and specificity.

In the majority of cases structural studies on nucleic acids using NMR spectroscopy do not allow determination of the location of bound cations. Similarly, the electron density obtained from crystallographic studies can be insufficient to unambiguously define type and location of ions bound to nucleic acids. The present study indicates that docking studies with a GB/FDPB continuum solvent approach allow systematic exploration of putative ion binding positions and are fast

enough to account for conformational changes during docking. Systematic applications to identify putative binding sites in various known structural motifs and large nucleic acid structures are possible.

ACKNOWLEDGEMENTS

We thank Dr Felipe Pineda for helpful comments and discussions. This work was supported by the Deutsche Forschungsgemeinschaft Grant ZA 153/3-1 to M.Z.

REFERENCES

1. Pyle,A.M. (1993) Ribozymes: a distinct class of metalloenzymes. *Science*, **261**, 709–714.
2. Wang,Y.X., Lu,M. and Draper,D.E. (1993) Specific ammonium ion requirement for functional ribosomal RNA tertiary structure. *Biochemistry*, **32**, 12279–12282.
3. Talbot,S. and Altman,S. (1994) Kinetic and thermodynamic analysis of RNA-protein interactions in the RNAse P holoenzyme from *Escherichia coli*. *Biochemistry*, **33**, 1406–1411.
4. Tinoco,I. and Kieft,J.S. (1997) The ion core in RNA folding. *Nature Struct. Biol.*, **4**, 509–512.
5. Cate,J.H., Gooding,A.R., Podell,E., Zhou,K., Golden,B.L., Kundrot,C.E., Cech,T.R. and Doudna,J.A. (1996) Crystal structure of a group I ribozyme domain: principles of RNA packing. *Science*, **273**, 1678–1685.
6. Cate,J.H., Gooding,A.R., Podell,E., Zhou,K., Golden,B.L., Szewczak,A.A., Kundrot,C.E., Cech,T.R. and Doudna,J.A. (1996) RNA tertiary structure mediation by adenosine platforms. *Science*, **273**, 1696–1699.
7. Cate,J.H., Hanna,R.L. and Doudna,J.A. (1997) A magnesium ion core at the heart of a ribozyme domain. *Nature Struct. Biol.*, **4**, 553–558.
8. Basu,S., Rambo,R.P., Strauss-Soukup,J., Cate,J.H., Ferré-D'Amaré,A., Strobel,S.A. and Doudna,J.A. (1998) A specific monovalent metal ion integral to the AA platform of the RNA tetraloop receptor. *Nature Struct. Biol.*, **5**, 986–992.
9. Batey,R.T., Rambo,R.P. and Doudna,J.A. (1999) Tertiary motifs in RNA structure and folding. *Angew. Chem. Int. Ed.*, **38**, 2326–2343.
10. Misra,V.K. and Draper,D.E. (1998) RNA shows its metal. *Nature Struct. Biol.*, **5**, 927–930.
11. Misra,V.K. and Draper,D.E. (1999) On the role of magnesium ions in RNA stability. *Biopolymers*, **48**, 113–135.
12. Guzman,R.N., Turner,R.T. and Summers,M.F. (1998) Protein-RNA recognition. *Biopolymers*, **48**, 181–195.
13. Cusack,S. (1999) RNA-protein complexes. *Curr. Opin. Struct. Biol.*, **9**, 66–73.
14. Cheatham,T.E.,III and Kollman,P.A. (1996) Observation of the A-DNA to B-DNA transition during unrestrained molecular dynamics in aqueous solution. *J. Mol. Biol.*, **259**, 434–444.
15. Feig,M. and Pettitt,B.M. (1998) A molecular simulation picture of DNA hydration around A- and B-DNA. *Biopolymers*, **48**, 199–209.
16. Feig,M. and Pettitt,B.M. (1999) Sodium and chlorine ions as part of the DNA solvation shell. *Biophys. J.*, **77**, 1769–1781.
17. Feig,M., Zacharias,M. and Pettitt,B.M. (2001) Conformation of an adenine bulge in a DNA octamer and its influence on DNA structure from molecular dynamics simulations. *Biophys. J.*, **81**, 352–370.
18. Auffinger,P. and Westhof,E. (1998) Simulation of the molecular dynamics of nucleic acids. *Curr. Opin. Struct. Biol.*, **8**, 227–236.
19. Zacharias,M. (2000) Simulation of the structure and dynamics of nonhelical RNA motifs. *Curr. Opin. Struct. Biol.*, **10**, 307–311.
20. Zacharias,M. (2000) Comparison of molecular dynamics and harmonic mode calculations on RNA. *Biopolymers*, **54**, 547–560.
21. Cheatham,T.E.,III and Kollman,P.A. (2000) Molecular dynamics simulations of nucleic acids. *Annu. Rev. Phys. Chem.*, **51**, 435–471.
22. Kollman,P.A., Massova,I., Reyes,C., Kuhn,B., Huo,S., Chong,L., Lee,M., Duan,Y., Wang,W., Donini,O., Cieplak,P., Srinivasan,J., Case,D.A. and Cheatham,T.E.,III (2000) Calculating structures and free energies of complex molecules: combining molecular mechanics and continuum models. *Acc. Chem. Res.*, **33**, 889–897.
23. Straatsma,T.P., Zacharias,M. and McCammon,J.A. (1993) Free energy difference calculations in biomolecular systems. In Van Gunsteren,W.F., Weiner,P.K. and Wilkinson,A.J. (eds), *Computer Simulation of Biomolecular Systems*. Escom Science Publishers, Leiden, NL, Vol. 2, pp 349–367.
24. Still,W.C., Tempczyk,A., Hawley,R.C. and Hendrikson,T. (1990) Semianalytical treatment of solvation for molecular mechanics and dynamics. *J. Am. Chem. Soc.*, **112**, 6127–6129.
25. Hawkins,G.D., Cramer,C.J. and Truhlar,D.G. (1995) Pairwise solute descreening of solute charges from a dielectric continuum. *Chem. Phys. Lett.*, **246**, 122–129.
26. Hawkins,G.D., Cramer,C.J. and Truhlar,D.G. (1996) Parametrized models of aqueous free energies of solvation based on pairwise descreening of solute atomic charges from a dielectric medium. *J. Phys. Chem.*, **100**, 19824–19839.
27. Jayaram,B., Sprous,D. and Beveridge,D.L. (1998) Solvation free energies of biomacromolecules: parameters for a modified generalized Born model consistent with the Amber force field. *J. Phys. Chem.*, **102**, 9571–9576.
28. Srinivasan,J., Miller,J., Kollman,P.A. and Case,D.A. (1998) Continuum solvent studies of the stability of RNA hairpin loops and helics. *J. Biomol. Struct. Dyn.*, **16**, 671–682.
29. Srinivasan,J., Trevathan,M.W., Beroza,P. and Case,D.A. (1999) Application of a pairwise generalized Born model to proteins and nucleic acids: inclusion of salt effects. *Theor. Chem. Acc.*, **101**, 426–434.
30. Zacharias,M. (2001) Conformational analysis of DNA-trinucleotide-hairpin-loop structures using a continuum solvent model. *Biophys. J.*, **80**, 2350–2363.
31. Williams,D.J. and Hall,K.B. (1999) Unrestrained stochastic dynamics simulations of the UUCG tetraloop using an implicit solvation model. *Biophys. J.*, **76**, 3192–3205.
32. Williams,D.J. and Hall,K.B. (2000) Experimental and theoretical studies of the effects of deoxyribose substitutions on the stability of the UUCG tetraloop. *J. Mol. Biol.*, **297**, 251–265.
33. Williams,D.J. and Hall,K.B. (2000) Experimental and computational studies of the G[UUCG]C RNA tetraloop. *J. Mol. Biol.*, **297**, 1045–1061.
34. Tsui,V. and Case,D.A. (2000) Molecular dynamics simulations of nucleic acids with a generalized Born solvation model. *J. Am. Chem. Soc.*, **122**, 2489–2498.
35. Sharp,K.A. and Honig,B. (1990) Calculating total electrostatic energies with the nonlinear Poisson-Boltzmann equation. *J. Phys. Chem.*, **94**, 7684–7692.
36. Lavery,R., Zakrzewska,K. and Sklenar,H. (1995) JUMNA (Junction minimization of nucleic acids). *Comput. Phys. Com.*, **91**, 135–158.
37. Cornell,W.D., Cieplak,P., Bayley,C.I., Gould,I.R., Merz,K.M., Ferguson,D.M., Spellmeyer,D.C., Fox,T., Caldwell,J.W. and Kollman,P. (1995) A second generation force field for simulation of proteins, nucleic acids and organic molecules. *J. Am. Chem. Soc.*, **117**, 5179–5197.
38. Aqvist,J.J. (1990) Ion-water interaction potential derived from free energy perturbation simulations. *J. Phys. Chem.*, **94**, 8021–8024.
39. Sitkoff,D., Sharp,K.A. and Honig,B. (1994) Accurate calculation of hydration free energies using macroscopic solvent models. *J. Phys. Chem.*, **98**, 1978–1988.
40. Madura,J.D., Davis,M.E., Wade,R., Luty,B.A., Ilin,A., Anosiewicz,A., Gilson,M.K., Bagheri,B., Ridgway-Scot,L. and McCammon,J.A. (1995) Electrostatics and diffusion of molecules in solution: simulations with University of Houston Brownian dynamics program. *Comput. Phys. Commun.*, **91**, 57–95.
41. Bondi,A. (1964) Van der Waals volumes and radii. *J. Phys. Chem.*, **64**, 441–451.
42. Burgess,M.A. (1978) *Metal Ions in Solution*. Ellis Horwood, Chichester, UK.
43. Shrake,A. and Rupley,J.A. (1973) Environment and exposure to solvent of protein atoms: lysozyme and insulin. *J. Mol. Biol.*, **79**, 351–365.
44. Butcher,S.E., Diekmann,T. and Feigon,J. (1997) Solution structure of a GAAA tetraloop receptor RNA. *EMBO J.*, **16**, 7490–7502.
45. Eisenman,G. (1962) Cation selective glass electrodes and their mode of operation. *Biophys. J.*, **2**, 259–323.
46. Eisenman,G. and Horn,R. (1983) Ion selectivity revisted: the role of kinetic and equilibrium processes in ion permeation through channels. *J. Membr. Biol.*, **76**, 197–225.
47. Hermann,T. and Westhof,E. (1998) Exploration of metal ion binding sites in RNA folds by brownian dynamics simulations. *Structure*, **6**, 1303–1314.
48. Zacharias,M. and Sklenar,H. (1999) Conformational analysis of single-base bulges in A-form DNA and RNA using a hierarchical approach and energetic evaluation with a continuum solvent model. *J. Mol. Biol.*, **289**, 261–275.
49. Rife,J.P., Stallings,S.C., Correl,C.C., Dallas,A., Steitz,T.A. and Moore,P.B. (1999) Comparison of the crystal and solution structures of two RNA oligonucleotides. *Biophys. J.*, **76**, 65–75.